JOURNAL OF RADIATION RESEARCH AND APPLIED SCIENCES
2020, VOL. 13, NO. 1, 507–514
https://doi.org/10.1080/16878507.2020.1756108

ARTICLE

OPEN ACCESS Check for updates

A modified semi-empirical formula to calculate the maximum positron range affected by different magnetic field strengths for PET/MRI scanner

Essam M. Banoqitah, Abdelfattah Y. Soliman, Eslam M. Taha and Abdelhamid K. Mazher

Nuclear Engineering Department, Faculty of Engineering, King Abdulaziz University, Jeddah, Saudi Arabia

ABSTRACT

A modified semi-empirical formula that relates the maximum range of the positron to the strength of different magnetic field strengths is developed via Monte Carlo simulation. The formula is derived as an extension to the existing formula of no magnetic field. COMSOL Multiphysics is used to simulate the different physics, including electromagnetic physics and charged particle tracking physics. The Monte Carlo simulation technique by COMSOL is employed to study the effect of magnetic field strength on the positron range PET/MRI scan of the head's tumor. The magnetic field varies in the range 1–10 Tesla. The simulation code using positron emission is conducted by the Monte Carlo method. Simulation results show that changing the magnetic field affects the particle trajectory and hence the maximum positron range. The elliptic trajectory causes a reduction in displacement between the original location of emission and the location of annihilation, which permits an increased photon emission per unit volume of the tumor and hence a better image resolution. The main contribution of the paper is the formulation of a new semi-empirical relation taking into account the presence of a magnetic field by simulating different particle trajectories for the different magnetic field strengths.

ARTICLE HISTORY
Received 19 October 2019
Accepted 11 April 2020

KEYWORDS
Positron range; MRI; PET; uncertainty; magnetic field

1. Introduction

Nuclear medicine is based on the administration of radiopharmaceuticals to the patients for diagnostic or treatment purposes. In diagnostic procedures, the patient is usually scanned using one of the two modalities: Single Photon Emission Computed Tomography 'SPECT' or Positron Emission Tomography 'PET.' Each modality has features and limitations that play a vital role in the produced image quality and thereby affect the assessment of patient condition and treatment.

SPECT and PET rely on the detection of photons to produce images illustrating the distribution of radionuclides in patients (Powsner & Powsner, 2006). One of the major differences between the two is the type of decay of the nuclide administered to the patient. SPECT utilizes gamma-emitting nuclides, whereas PET uses positron-emitting nuclides. Gamma photons emitted from the patient are directly detected by a gamma camera after passing a collimator that preserves resolution to some extent.

In PET, a positron travels some distance before combining with an electron producing pair of annihilation photons. When paired annihilation photons are detected, it is possible to identify the site from which they originated. Locating the point of origin for annihilation events serves as the foundation in producing tomographic images in PET (Bushberg et al., 2012).

The distance traveled by a positron before undergoing annihilation poses a limitation to resolution. The positron shift from the point of emission to the point of annihilation production causes some blurring that hinders image resolution. This blurring is affected by positron energy and tissue composition (Cho et al., 1975; Levin & Hoffman, 1999; Sánchez-Crespo et al., 2004). Cal-González et al. used the PeneloPET simulation toolkit to determine the positron range in different materials and for different radioisotopes and proposed a scaling method to estimate the positron range for any isotope/material combination (Cal-González et al., 2013).

Several studies have been carried out to evaluate the resolution loss due to the positron range. Matthew et al. developed a model predicting positron range distributions and the consequent imaging system resolution loss. The study suggested a possibility of blurring correction during iterative reconstruction (Palmer & Brownell, 1992; Palmer et al., 2005). Nowadays, almost all PET systems are coupled either to computed tomography (CT) or magnetic resonance imaging system (MRI) (Huang et al., 2016; Zaidi & Del Guerra, 2011). Each of those complementary systems adds a distinct feature to PET while there is a limitation (Burgos et al., 2014; Bushberg et al., 2012; Huang et al., 2016; Zaidi & Del Guerra, 2011).

Several types of research were interested in studying the effect of a magnetic field on the positron range. Iida et al., showed positrons annihilation probability to increase from 0.13 to 0.23 in a 1 mm diameter cylinder when a magnetic field 5 Tesla is applied. The probability

CONTACT Essam M. Banoqitah ebanoqitah@kau.edu.sa

is further increased to 0.50 with 10 Tesla (Iida et al., 1986). In another Monte-Carlo study, Raylman et al., showed an approximate 27% improvement in PET resolution when a magnetic field of 10 Tesla is incorporated (Raylman et al., 1996). In these research efforts, the magnetic field was constant up to 10 Tesla, and it's assumed to be uniform all over the geometry and not affected by the presence of the head.

The use of the magnetic flux density from MRI to reduce the maximum positron range in PET scan will be investigated in work herein. In the present research, the Monte Carlo simulation method is employed to study the effect of a different magnetic field on the positron range in tumors. The head and the tumor model are constructed using COMSOL Multiphysics, where the finite element method used for magnetic field calculations and the Monte Carlo method for particle transport. The construction of a 3D magnetic field that varies with the position and affected by the presence of the patient head will give an accurate simulation of its effect on the positrons trajectories.

2. Model description and calculation methodology

The finite element method is employed using COMSOL Multiphysics software to construct the geometry of a patient's head model. The head model consists of episodes that represent the skin, skull, and soft brain tissue, each with different magnetic properties due to the difference in electric conductivity and relative permeability, see Figure 1. The head model was located 30 cm away from the coil center. A static magnetic field was constructed using a coil to generate a magnetic field inside the model of the patient head, which includes a tumor at its center, see Figure 2.

Ampere's law is used to drive the magnetostatic equation for a 3D static magnetic field surrounding the coil, as stated in Equation (1).

$$\nabla \times \left(\mu_o^{-1}\mu_r^{-1}B\right) - \sigma v \times B = J_e; \quad B = \nabla XA \tag{1}$$

Where;

σ is the electric conductivity

μ_o is the permeability constant

μ_r is the relative permeability

A is the magnetic vector potential and $\mathbf{u} \times A = 0$ for the insulators, and **u** is a unit vector normal to the surface of the insulator (a tangential component of the magnetic potential is zero)

J_e is an externally generated current density

v is the velocity

B is the magnetic flux density in Tesla (T)

For a circular coil of current I_{coil} in Amperes (A), the number of turns N, the coil current flow $e_{coil,}$ and the cross-section area **S**, the current density is calculated using Equation (2).

$$J_e = \frac{NI_{coil}}{S} e_{coil} \tag{2}$$

Positrons are allowed to be emitted from the center of the tumor and subjected to magnetic force, as shown in Equation (3).

$$F_t = Ze(v \times B) = \frac{d(m_p v)}{dt} \tag{3}$$

Where;

Z is the charge number (z = 1 for positron)

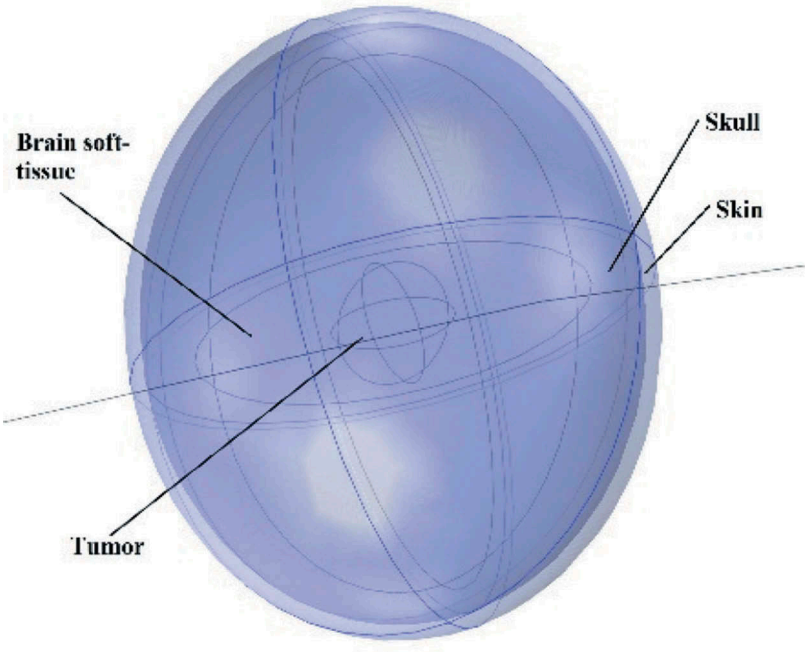

Figure 1. Patient' head model.

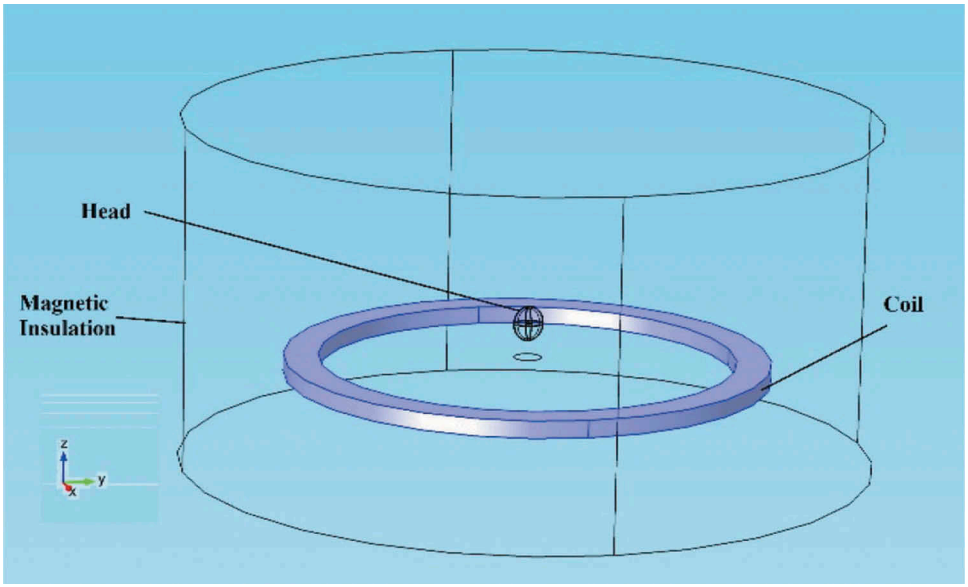

Figure 2. Model layout.

e is the electron charge
m_p is the positron mass
v is positron velocity
F_t total magnetic force

COMSOL Multiphysics charged particle tracking module is used to simulate the charged particle histories. Monte Carlo codes are based on averaging the particle behavior by generating many histories to simulate the particle tracks inside the material. The tallying by averaging the counting statistics may cause the loss of track information. In our case, different tracks are very sensitive to the presence of the magnetic field, which may deflect the trajectories of the particles in space. Furthermore, most of the commercial Monte Carlo codes don't permit a description of the detailed magnetic flux distribution

Monte Carlo algorithm was constructed to investigate the effect of the magnetic field on the positron range. This algorithm is based on creating just one history to represent one positron at a time. This positron is allowed to move a complete range by adjusting the total cross section of the medium and time cut off for the problem. The angle dependence of the magnetic field causes charged particles to move perpendicular to the magnetic field lines in a circular or helical motion, which causes a reduction in displacement between the original location of emission and the location of annihilation. The number of photons emitted per unit volume of the tumor will be increased due to this reduction in the displacement and permits a better image resolution.

The magnetic field doesn't cause a gain in energy, and it just decreases with the angle between the normal magnetic flux density and the velocity vector because the magnetic force changes the velocity vector by changing its direction without affecting its magnitude. Many histories are generated to represent an isotropic source of positrons, and the particle trajectories are investigated.

The maximum positron range, according to the semi-empirical relationship of Evans (EVANS, 1972), is given by Equation (4) for a given maximum positron energy E_β^{max} and for a given medium of density ρ.

$$R_{max}(cm) \simeq \frac{412\left[E_\beta^{max}(MeV)\right]^n}{\rho(mgcm^{-3})}; 0.01 \leq E_\beta^{max} \leq 2.5MeV; \quad n = 1.255 - 0.0954ln\left[E_\beta^{max}(MeV)\right] \tag{4}$$

The total positron interaction mean free path is given by Equation (5), where σ is the total cross section, N_D is the atom density, A_m is the mixture atomic weight, λ is the mean free path and N_A is Avogadro's number.

$$\lambda = \frac{1}{N_D\sigma} = \frac{A_m}{\rho(g/cm^3).N_A\sigma} \tag{5}$$

Assuming that all positrons are emitted isotopically with a mean free path equal the maximum range, the semi-empirical formula (4) could be deduced from Equations (5), (6) and (7).

$$\lambda_e \approx R_{max} \tag{6}$$

$$\sigma = \frac{10^{-3}.A_m}{412.N_A.\left[E_\beta^{max}(MeV)\right]^n} \tag{7}$$

A Monte Carlo simulation was done to permit the creation of isotropic positrons histories in the tumor center of an interaction cross section corresponds to Equation (7). Time cut off is used to simulate the furthest distance by these positrons and to simulate the maximum particle range. The time cut off is defined as the time required by one history to cross a distance equal to the maximum positron range, as shown in Equation (8). If all the positrons are monoenergetic, they will cross a distance of $\boldsymbol{R_{max}}$ within time T_{max}.

$$T_{max} \approx \frac{R_{max}(cm)}{\sqrt{\frac{2E_{\beta}^{max}}{m_p}}} \quad (8)$$

The main idea behind creating the histories that way is to simulate the maximum particle range for different particle trajectories and material compositions. If any material of A_m is simulated for any positron energy, the maximum range of this material will have the same value as predicted by Evans relation (4).

3. Results and discussions

The finite element method is used to create a stationary magnetic field for the whole geometry, including the coil, head, tumor, and the surrounding air, as shown in Figure 3. The magnetic flux density is calculated in the entire geometry for various coil currents. Figure 4 shows the magnetic flux density at for current value of 1.5 A. As the coil current change, the magnetic flux density at the tumor and the surrounding will change. The magnetic flux density as a function of the coil current at the tumor center is shown in Figure 5. It is clear that the magnetic flux density at the tumor center is directly proportional to the coil current. It's expected that varying the head position along the coil axis will decrease or increase the magnetic flux density, and no further studies are needed for different head positions since changing the position will require adjusting the current to get the same magnetic flux density at the tumor center. Magnetic field lines through the 3D geometry are shown in Figure 6, and the magnetic flux density at the x-y plane is shown in Figure 7. The magnetic flux density B for a current of 950 A, inside the model head of the patient, was around 9.5 T, according to the model geometry, see Figure 8.

Simulations were done for magnetic flux densities (B) from 0 to 10 T. A unit vector s, in r direction, is taken to allow the calculation of range in different directions relative to normal B. The magnetic field will affect the trajectories of the particles, which will alter the $\boldsymbol{R_{max}}$ according to

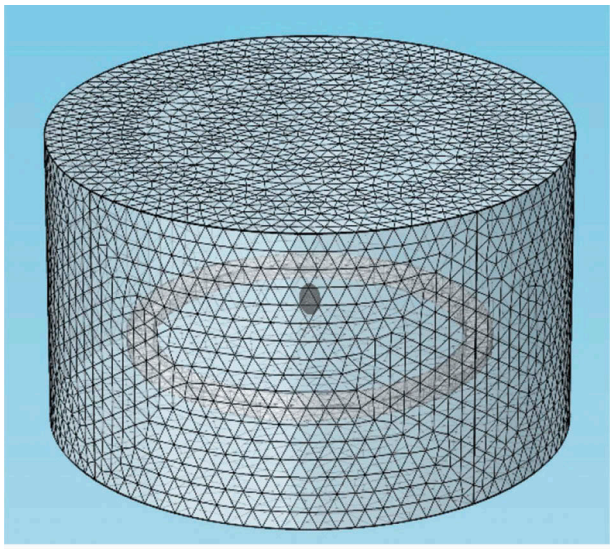

Figure 3. Extra fine mesh structure.

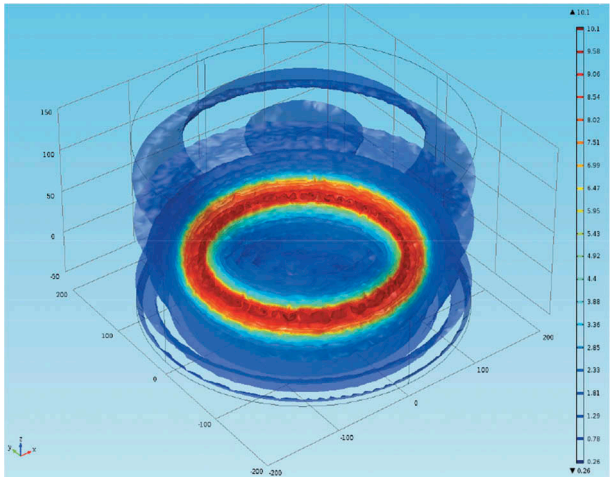

Figure 4. 3D magnetic flux density surrounding the coil for coil current 1.5 A.

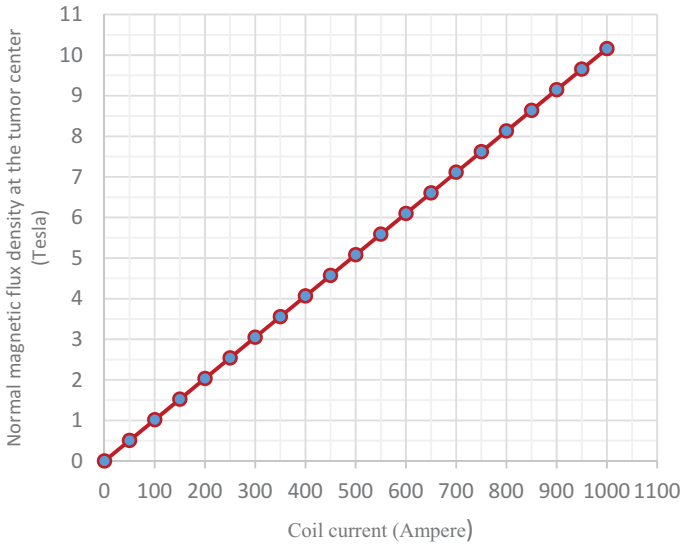

Figure 5. Relation between magnetic flux density at tumor center and coil current.

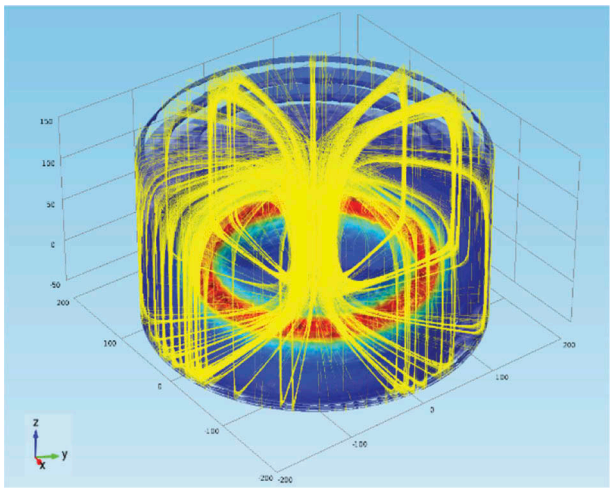

Figure 6. Magnetic field lines.

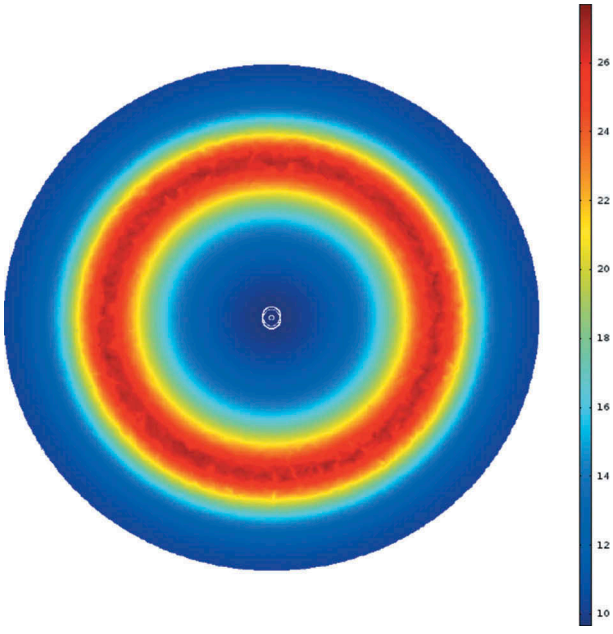

Figure 7. Normal magnetic flux density at the x-y plane.

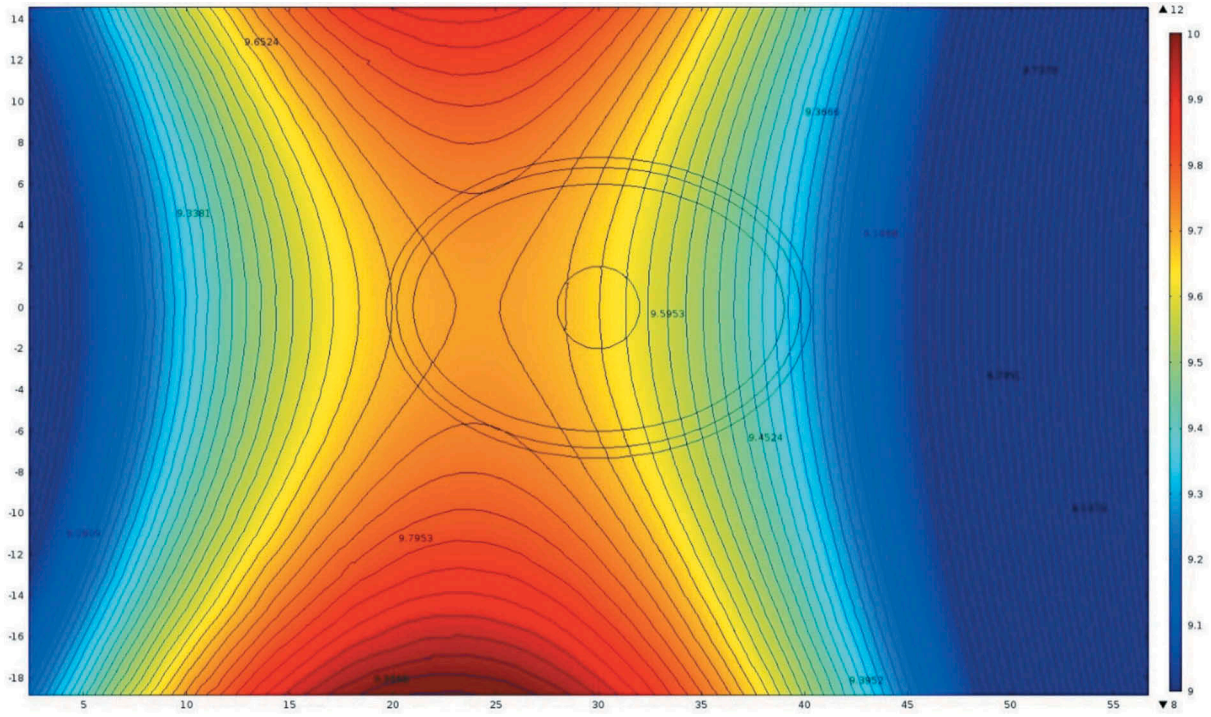

Figure 8. Normal magnetic flux density for coil current of 950 Ampere.

the 3D distribution of the magnetic flux density. If the magnetic flux density changes the particle trajectory, the history will be terminated before reaching $\boldsymbol{R_{max}}$ for the same cut off time. Figure 9 shows the positrons' histories in the absence of a magnetic field, and it is noticed that all the particles reach $\boldsymbol{R_{max}}$, as defined by Evans. Figure 10 shows the particles 3D $\boldsymbol{R_{max}}$ distributions in the presence of a magnetic flux density of 9.65 T. A remarkable contraction of the maximum range in the tumor planes parallel to the coil plane. Due to the presence of a magnetic field, the 3D profile changes from spherical shape to an ellipsoid shape with contraction in x and y directions.

The effect of the magnetic field is used to deduce a modified semi-empirical relation taking into account the presence of a magnetic field by simulating different particle energies and varying magnetic field strengths, Equation (9). Data from the simulations are used to add another term to the Evans equation, and this term represents the effect of the presence of the magnetic field on the 3D positron range. The $\boldsymbol{R_{max}}$ contraction according to the simulations and the deduced semi-empirical formula in a plane parallel to the coil plane. Figure 11 shows the variation of $\boldsymbol{R_{max}}$ for different magnetic flux and positron sources. The plane parallel to the coil plane has the maximum contraction because the velocity vectors are normal to the magnetic flux density norm.

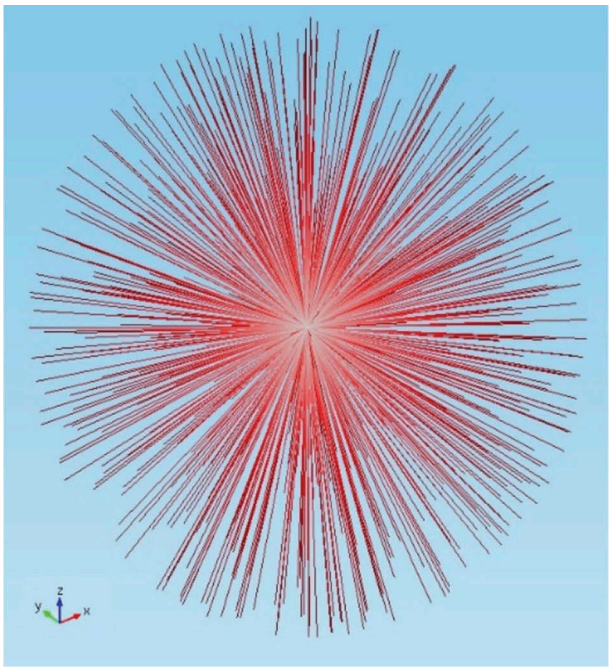

Figure 9. Particles trajectories (B = 0 T).

$$R_{max}(cm) \simeq \frac{412\left[E_\beta^{max}(MeV)\right]^n}{\rho(mgcm^{-3})}\left\{1.068e^{-0.2771\left|\vec{B}\times\vec{r}\right|} - 0.068e^{-10^6\left|\vec{B}\times\vec{r}\right|}\right\};$$
$$n = 1.255 - 0.0954ln\left[E_\beta^{max}(MeV)\right];$$
$$0.01 \le E_\beta^{max} \le 2.5MeV \tag{9}$$

Where $\vec{r}$is a unit vector in the positron direction.

The modified semi-empirical formula shows that the maximum positron range decreases with

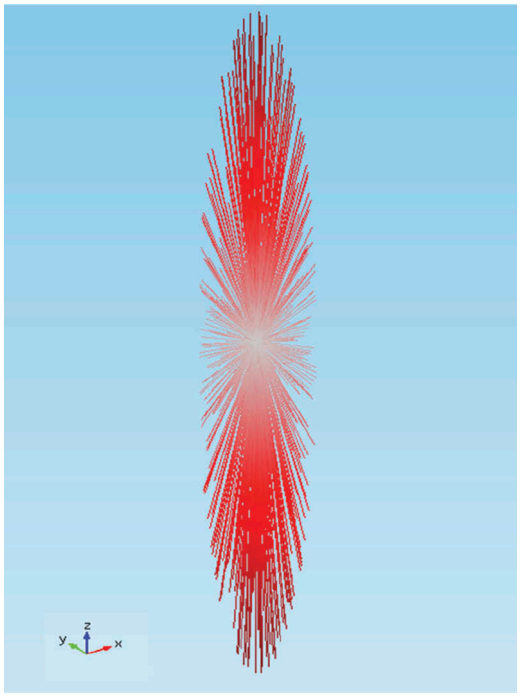

Figure 10. Particles trajectories (B = 9.65 T).

increasing the magnetic flux density at the patient's head for different positron-emitting isotopes. A significant reduction in R_{max} is observed by increasing the magnetic field density. Table 1 shows the required magnetic field intensity required to reduce R_{max} below 1 mm for different positron emitters sources. F-18 shows the minimum required magnetic flux density at the tumor

Table 1. Required magnetic field to reduce R_{max} below 1 mm.

Isotope	R_{max} at T = 0	Required magnetic field density for R_{max} < 1 mm	Percentage reduction of R_{max}
F-18	2.08	3	108
C-11	3.53	5	253
N-13	4.69	6	370
O-15	7.63	8	663
Ga-68	8.72	9	771
Rb-82	15.89	10	1449

to reduce R_{max} below 1 mm because its initial R_{max} with the absence of the magnetic field is the lowest among the other isotopes. The lower magnetic flux density required with F-18 means less cooling for the coil and high image resolution at the same time.

4. Conclusion

Coupling of electromagnetics and particle tracking using COMSOL Multiphysics enables updating a semi-empirical formula to calculate the maximum positron range under the influence of different magnetic field strengths. A significant reduction in the maximum positron range with increasing the magnetic flux density for different positron-emitting isotopes.F-18 shows the minimum required magnetic flux density of about 3 T to reduce R_{max} below 1 mm by a percentage reduction of 108%. Other positron-emitting isotopes such as C-11, N-13, O-15, G-68, and Rb-82 require a magnetic flux intensity ranges between 5 to 10 T to reduce R_{max} below 1 mm.

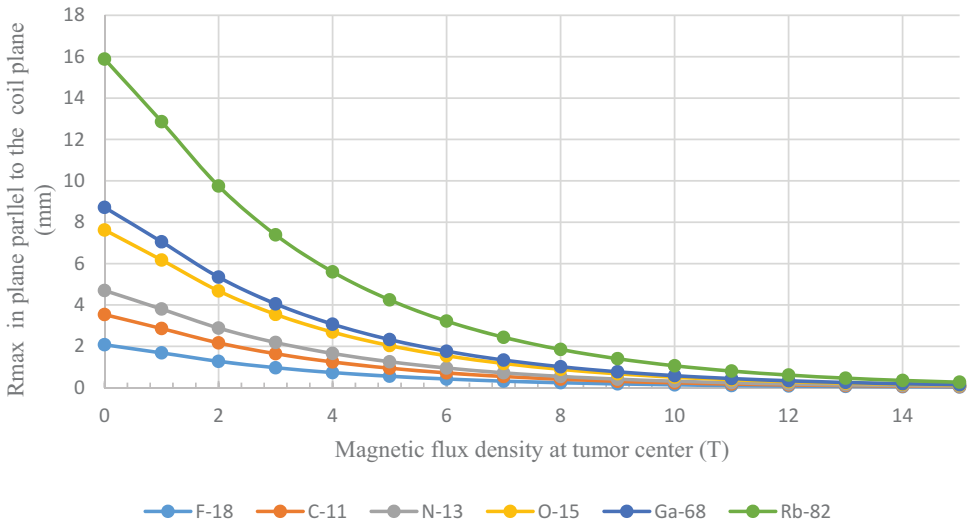

Figure 11. R_{max} for different magnetic flux densities at a plane parallel to the coil plane for different positron sources.

Disclosure statement

No potential conflict of interest was reported by the authors.

Funding

This work was supported by the King Abdulaziz University [135-951-D1435].

ORCID

Essam M. Banoqitah http://orcid.org/0000-0002-9127-6322
Abdelfattah Y. Soliman http://orcid.org/0000-0002-4831-9251
Eslam M. Taha http://orcid.org/0000-0002-1867-4703

References

Burgos, N., Cardoso, M. J., Thielemans, K., Modat, M., Pedemonte, S., Dickson, J., Barnes, A., Ahmed, R., Mahoney, C. J., Schott, J. M., Duncan, J. S., Atkinson, D., Arridge, S. R., Hutton, B. F., & Ourselin, S. (2014). Attenuation correction synthesis for hybrid PET-MR Scanners: Application to Brain Studies. *IEEE Transactions on Medical Imaging*, *33*(12), 2332–2341. https://doi.org/10.1109/TMI.2014.2340135

Bushberg, J. T., Seibert, J. A., Leidholdt, E. M., Boone, J. M., & Goldschmidt, E. J. (2012). The essential physics of medical imaging. In *Medical physics* (3rd ed., Vol. 30), pp. 1048. LWW; Third, North American edition. https://doi.org/10.1118/1.1585033

Cal-González, J., Herraiz, J. L., España, S., Corzo, P. M. G., Vaquero, J. J., Desco, M., & Udias, J. M. (2013). Positron range estimations with PeneloPET. *Physics in Medicine and Biology*, *58*(15), 5127–5152. https://doi.org/10.1088/0031-9155/58/15/5127

Cho, Z. H., Chan, J. K., Ericksson, L., Singh, M., Graham, S., MacDonald, N. S., & Yano, Y. (1975). Positron ranges obtained from biomedically important positron-emitting radionuclides. *Journal of Nuclear Medicine: Official Publication, Society of Nuclear Medicine*, *16*(12), 1174–1176. https://www.ncbi.nlm.nih.gov/pubmed/1194970

EVANS, R. T. atomic nucleus. (1972). *Statical fluctuations in nuclear processes*. McGraw-Hill.

Huang, S. Y., Savic, D., Yang, J., Shrestha, U., & Seo, Y. (2016). The effect of magnetic field on positron range and spatial resolution in an integrated whole-body time-of-flight PET/MRI system. *2014 IEEE Nuclear Science Symposium and Medical Imaging Conference, NSS/MIC 2014*, *94143*, 1–4. https://doi.org/10.1109/NSSMIC.2014.7431006

Iida, H., Kanno, I., Miura, S., Murakami, M., Takahashi, K., & Uemura, K. (1986). A simulation study of a method to reduce positron annihilation spread distributions using a strong magnetic field in positron emission tomography. *IEEE Transactions on Nuclear Science*, *33*(1), 597–600. https://doi.org/10.1109/TNS.1986.4337173

Levin, C. S., & Hoffman, E. J. (1999). Calculation of positron range and its effect on the fundamental limit of positron emission tomography system spatial resolution. *Physics in Medicine and Biology*, *44*(3), 781. https://doi.org/10.1088/0031-9155/44/3/019

Palmer, M. R., & Brownell, G. L. (1992). Annihilation density distribution calculations for medically important positron emitters. *IEEE Transactions on Medical Imaging*, *11*(3), 373–378. https://doi.org/10.1109/42.158941

Palmer, M. R., Zhu, X., & Parker, J. A. (2005). Modeling and simulation of positron range effects for high-resolution PET imaging. *IEEE Transactions on Nuclear Science*, *52*(5), 1391–1395. https://doi.org/10.1109/TNS.2005.858264

Powsner, R. A., & Powsner, E. R. (2006). *Essential nuclear medicine physics* (R. A. Powsner & E. R. Powsner, Eds.). Blackwell Publishing Ltd. https://doi.org/10.1002/9780470752890

Raylman, R. R., Hammer, B. E., & Christensen, N. L. (1996). Combined MRI-PET scanner: A Monte Carlo evaluation of the improvements in PET resolution due to the effects of a static homogeneous magnetic field. *IEEE Transactions on Nuclear Science*, *43*(4), 2406–2412. https://doi.org/10.1109/23.531789

Sánchez-Crespo, A., Andreo, P., & Larsson, S. A. (2004). Positron flight in human tissues and its influence on PET image spatial resolution. *European Journal of Nuclear Medicine and Molecular Imaging*, *31*(1), 44–51. https://doi.org/10.1007/s00259-003-1330-y

Zaidi, H., & Del Guerra, A. (2011). An outlook on future design of hybrid PET/MRI systems. *Medical Physics*, *38*(10), 5667–5689. https://doi.org/10.1118/1.3633909